

Temperature-dependent Faraday rotation and magnetization reorientation in cerium-substituted yttrium iron garnet thin films

Enno Lage, Lukas Beran, Andy Udo Quindeau, Lukas Ohnoutek, Miroslav Kucera, Roman Antos, Sohrab Redjai Sani, Gerald F. Dionne, Martin Veis, and Caroline A. Ross

Citation: *APL Materials* **5**, 036104 (2017); doi: 10.1063/1.4976817

View online: <http://dx.doi.org/10.1063/1.4976817>

View Table of Contents: <http://aip.scitation.org/toc/apm/5/3>

Published by the [American Institute of Physics](#)

Articles you may be interested in

[Pulsed laser deposition of epitaxial yttrium iron garnet films with low Gilbert damping and bulk-like magnetization](#)

APL Materials **2**, 106102 (2014); 10.1063/1.4896936

[Spin-wave propagation in ultra-thin YIG based waveguides](#)

Applied Physics Letters **110**, 092408 (2017); 10.1063/1.4976708

[Epitaxial growth of \$Y_3Fe_5O_{12}\$ thin films with perpendicular magnetic anisotropy](#)

Applied Physics Letters **110**, 202403 (2017); 10.1063/1.4983783

[Fast switching and signature of efficient domain wall motion driven by spin-orbit torques in a perpendicular anisotropy magnetic insulator/Pt bilayer](#)

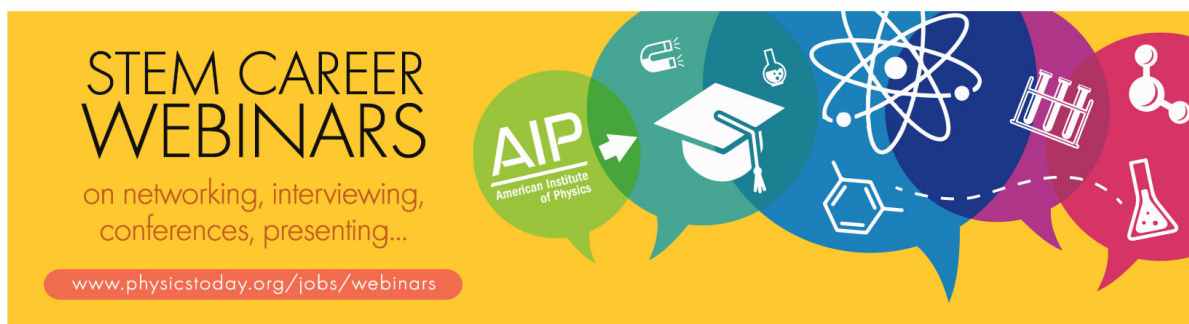
Applied Physics Letters **111**, 072406 (2017); 10.1063/1.4994050

[Magnetic, electronic, and optical properties of double perovskite \$Bi_2FeMnO_6\$](#)

APL Materials **5**, 035601 (2016); 10.1063/1.4964676

[Spin Seebeck effect in insulating epitaxial \$\gamma\$ - \$Fe_2O_3\$ thin films](#)

APL Materials **5**, 026103 (2017); 10.1063/1.4975618



STEM CAREER WEBINARS

on networking, interviewing, conferences, presenting...

www.physicstoday.org/jobs/webinars

AIP American Institute of Physics

The banner features a series of overlapping speech bubbles in various colors (green, blue, purple, red) containing icons related to science and education: a graduation cap, a microscope, a beaker, a test tube, a molecular structure, and a lightbulb. The AIP logo is prominently displayed in a green bubble on the left.

Temperature-dependent Faraday rotation and magnetization reorientation in cerium-substituted yttrium iron garnet thin films

Enno Lage,¹ Lukas Beran,² Andy Udo Quindeau,¹ Lukas Ohnoutek,² Miroslav Kucera,² Roman Antos,² Sohrab Redjai Sani,¹ Gerald F. Dionne,¹ Martin Veis,² and Caroline A. Ross¹

¹Department of Materials Science and Engineering, Massachusetts Institute of Technology, Cambridge, Massachusetts 02139, USA

²Charles University of Prague, Faculty of Mathematics and Physics, Ke Karlovu 3, 12116, Prague 2, Czech Republic

(Received 19 September 2016; accepted 26 January 2017; published online 10 March 2017)

We report on the temperature dependence of the magnetic and magneto-optical properties in cerium-substituted yttrium iron garnet (Ce:YIG) thin films. Measurements of the Faraday rotation as a function of temperature show that the magnetic easy axis of thin Ce:YIG films reorients from in-plane to out-of-plane on cooling below -100 °C. We argue that the temperature-dependence of the magnetostriction and magnetocrystalline anisotropy of Ce:YIG is the dominant factor contributing to the change in easy axis direction, and we describe the changes in the magneto-optical spectra with temperature. © 2017 Author(s). All article content, except where otherwise noted, is licensed under a Creative Commons Attribution (CC BY) license (<http://creativecommons.org/licenses/by/4.0/>). [<http://dx.doi.org/10.1063/1.4976817>]

Faraday rotation (FR) is observed when the magnetic field in a magneto-optical (MO) material is parallel to the Poynting vector of the transmitted light.¹ Yttrium iron garnets (YIG, $Y_3Fe_5O_{12}$)² when substituted with cerium (Ce:YIG, $(Ce,Y)_3Fe_5O_{12}$)^{3,4} or other elements such as Bi^{5,6} possess a high figure of merit (FR/optical absorption) at near-infrared communications wavelengths and are therefore well suited for making nonreciprocal optical devices.^{2,7-9} Thin films of Ce:YIG have been epitaxially grown by various deposition techniques on gallium gadolinium garnet (GGG) substrates^{10,11} or as polycrystalline films on silicon-based substrates.^{3,12,13} These polycrystalline and epitaxial films usually show an in-plane easy axis, though a domain structure with out-of-plane remanence has been revealed in epitaxial Ce:YIG films using polar magneto-optical Kerr effect measurements.² Other doped garnets show an anisotropy that can be adjusted via a thickness-dependent strain.¹⁴

The effects of the composition¹⁵⁻¹⁸ and processing conditions^{3,19,20} on the properties of substituted YIG have been widely explored with respect to maximizing the FR. However, investigation of the temperature-dependence of the MO and magnetic properties of Ce:YIG is limited and mostly focused on bulk materials.²¹⁻²⁴ Temperature-dependent studies of bulk Ce:YIG demonstrate an increase of saturation magnetization²² and Faraday rotation²¹ upon cooling which is well approximated by a linear function in the regime from room temperature (RT) to liquid nitrogen temperature. There are little data on magnetocrystalline anisotropy or magnetostriction of Ce:YIG, but rare earth iron garnets typically show a monotonic increase of the magnetocrystalline anisotropy by a factor of 5–50 and an increase in magnetostriction coefficients by a factor of 2–5 when cooled down from RT to liquid nitrogen temperatures.^{25,26} Previous studies of the magnetostriction of Ce:YIG show that Ce^{3+} ions contribute to a positive magnetostrictive coefficient. However, the investigations are limited to small Ce concentrations.^{23,24} The temperature-dependence of the optical properties of garnets is important in the operation of optical imaging devices, isolators, or sensors.^{27,28} Investigations of FR in the low temperature regime have been carried out for various iron garnets²⁹⁻³¹ and indicate a higher FR at low temperatures. Ce^{3+} ions contribute to a significant enhancement of the FR at low temperatures in Ce:YIG.²⁹

In this article, we examine the temperature dependence of the properties of Ce:YIG films on GGG substrates, including the lattice dimensions and strain, the coercivity, saturation field, and the wavelength-dependent FR. We show that the Ce:YIG films exhibit a magnetization reorientation transition which is discussed in terms of the anisotropy contributions.

The Ce:YIG films were grown by pulsed laser deposition (PLD) on 1 cm² double-side polished GGG (111) substrates, using a KrF excimer laser (wavelength 248 nm) with 10 Hz, 25 ns pulses. The base pressure was 5×10^6 Torr and the deposition pressure 5×10^{-3} Torr oxygen. The target was prepared from Y₂O₃, Fe₂O₃, and CeO₂ powders by a mixed oxide sintering method.^{3,32} The samples were grown with a target-sample distance of 5 cm and a substrate temperature of 650 °C. After deposition, the samples were cooled down at 5×10^{-3} Torr with a cooling rate of 15 °C/min. During deposition, the target and samples were rotated to ensure a homogenous ablation and uniform growth. The film composition and thickness were measured by means of wavelength dispersive X-ray spectroscopy (WDS) and X-ray reflectometry (XRR), respectively (data not shown). The film composition was Ce_{0.59±0.18}Y_{2.86±0.41}Fe_{4.55±0.5}O₁₂ based on the cation ratios, i.e., the film showed an iron deficiency likely to be caused by the target's surface modification,³² and the thickness was close to 80 nm.

Reciprocal space maps (RSMs) were obtained at RT, and Θ -2 Θ X-ray diffraction (XRD) scans were obtained in a range from -175 °C to +25 °C. The RSM of the (642) peaks (Fig. 1(a)) indicates that the Ce:YIG is well matched in-plane to the GGG lattice (bulk lattice parameter 12.383 Å) with minor strain relaxation in the Ce:YIG which is indicated by a broadening of the diffraction peak of the Ce:YIG towards lower q_x values and higher q_z values that correspond to a less strained unit cell. The out-of-plane d_{444} of the film is larger than the in-plane lattice spacing (out-of-plane: $4\sqrt{3}d_{444} = 12.52$ Å) and indicates that the Ce:YIG lattice is rhombohedrally distorted, with tensile strain along the [111] direction and compressive strain in-plane. This is in agreement with a

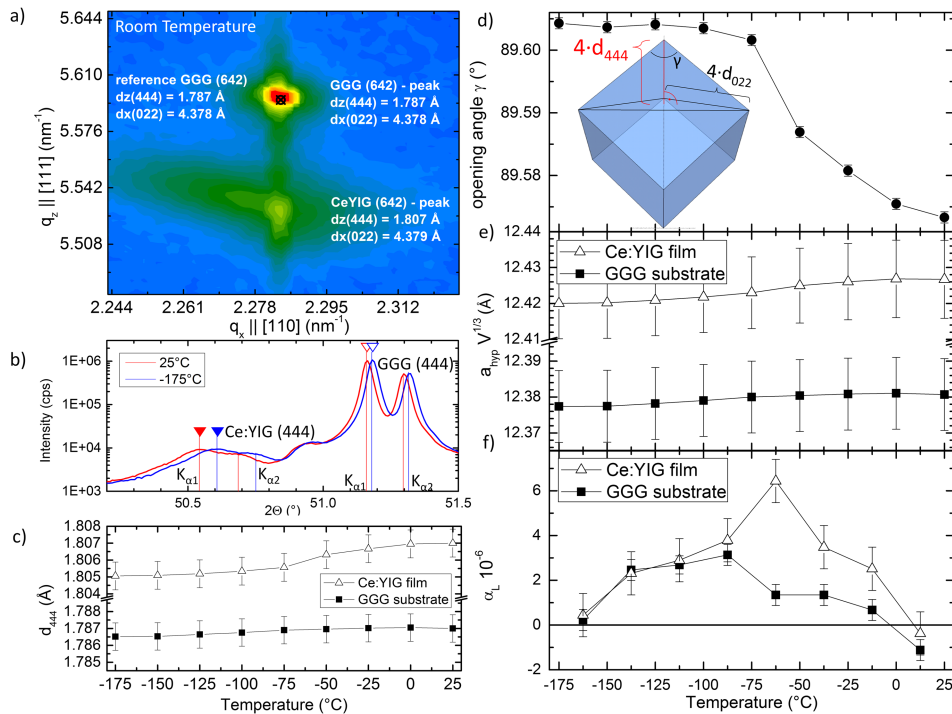


FIG. 1. X-ray structural analysis of Ce:YIG/GGG. (a) The reciprocal space map obtained at RT indicates in-plane lattice matching between GGG and Ce:YIG. Reference data for bulk GGG is shown as a black square. (b) The 2 Θ -scans at +25 °C and -175 °C show a temperature-dependent peak shift to higher angles which is more pronounced for the film (filled markers) compared to the GGG substrate (open markers). (c) The d_{444} out-of-plane lattice spacing of the film and substrate as a function of temperature. (d) The calculated facet angle γ of the rhombohedrally distorted unit cell. (e) The calculated lattice constant for GGG and the pseudocubic lattice constant for Ce:YIG. (f) The linear expansion coefficient of the film and substrate.

previous report.³ The lattice parameter reported for bulk material of comparable composition is $12.44 \pm 0.01 \text{ \AA}$.³³

The Θ - 2Θ -scans (Fig. 1(b)) show that the GGG (444) peaks (Cu $K_{\alpha 1}$ and corresponding Cu $K_{\alpha 2}$ doublets) shift by $\sim 0.01^\circ$ and the Ce:YIG (444) peaks shift by $\sim 0.025^\circ$ over the temperature range. The unshifted feature around 50.9° is an artifact due to the absorption edge of the Ni filter which is mounted in front of the detector and is hence unaffected by the cryostat temperature. The unit cell of the strained Ce:YIG is a rhombohedrally distorted cube whose facets have angles γ and $(180^\circ - \gamma)$, with γ representing the facet angles that meet along the [111] out-of-plane direction. The unit cell volume and γ are calculated from the geometry of the three-sided pyramid shown in Fig. 1(d), where the in-plane [011] lattice parameter of Ce:YIG is assumed equal to that of GGG [011] and the height is determined from d_{444} of Ce:YIG measured from XRD. This tetrahedron constitutes 1/6 of the unit cell volume which is given by $V = a^3(1 - 3\cos^2\gamma + 2\cos^3\gamma)^{0.5}$, from which γ is found. At RT, $\gamma = 89.57^\circ$ which implies in-plane compressive strain, also evident from the RSM (Fig. 1(a)). For lower temperatures, the GGG is assumed to remain cubic so its d_{444} lattice spacing (Fig. 1(c)) can be used to calculate the d_{220} in-plane spacing of the substrate and hence of the epitaxially grown film. The variation of γ with temperature is presented in Fig. 1(d) and shows a value consistently lower than 90° , indicating compressive stress. From RT to around -75°C , γ increases on cooling from 89.57° to 89.60° , but below -75°C there is little temperature dependence. The increase of γ towards 90° implies a decreasing in-plane compressive stress at lower temperatures.

Fig. 1(e) shows the lattice parameter of GGG and the pseudocubic lattice parameter for the Ce:YIG, a_{hyp} calculated as $V(T)^{1/3}$. The Ce:YIG/GGG mismatch is greatest at RT and decreases with temperature. The thermal expansion coefficient was determined as the difference between the pseudocubic lattice parameters ($a_{\text{hyp},T2} - a_{\text{hyp},T1}$) with respect to their average $(a_{\text{hyp},T2} + a_{\text{hyp},T1})/2$ for consecutive measurements at temperatures T1 and T2. The Ce:YIG film has a higher thermal expansion coefficient than GGG for $T > -100^\circ\text{C}$, with a maximum of $\sim 6 \times 10^{-6}$ at -75 to -50°C , but the two materials show similar expansion coefficients of $\sim 3 \times 10^{-6}$ at lower temperatures (in Fig. 1(f)) which agrees with a previously reported value of 3.35×10^{-6} for GGG.³⁴

Measurements of FR vs. temperature were made by mounting the double-side polished samples to a temperature-controlled microscopy stage (Linkam Scientific FTIR 600) with magnetic field perpendicular to the sample surface following the setup described in Ref. 35. The obtained FR loops are shown in Figure 2(a) for selected temperatures of $+25^\circ\text{C}$, -100°C , and -195°C after background subtraction. The wavelength of 1550 nm was selected for its relevance to telecommunication applications. The saturation FR varies from 3500°cm^{-1} at RT to $\sim 7800^\circ\text{cm}^{-1}$ at -195°C . The variation with temperature (Fig. 2(b)) shows an increase of a factor around 2.2 which is below previously reported values for lower Ce content $\text{Ce}_{0.045}\text{Y}_{2.955}\text{Fe}_5\text{O}_{12}$.²¹ The errors bars in Fig. 1 result from a (propagated) uncertainty of $\Delta\Theta = 0.001^\circ$.

Notably, the FR loops suggest a magnetization reorientation, in which the easy axis lies in-plane at RT but out-of-plane at -195°C . The gradual transition is exemplified by the measurement obtained at -100°C . The increasing coercivity with decreasing temperature is presented in Fig. 2(c). The out-of-plane saturation field, H_{sat} , was determined from the Faraday loops as shown in Fig. 2(a). Above -100°C , the FR loops were characteristic of a hard axis with low coercivity ($\mu_0 H_c < 10 \text{ mT}$), suggesting that the easy axis is in-plane. Below -100°C , the FR loops have high remanence and coercivity and suggest an out-of-plane easy axis. The saturation fields were $\sim 50 \text{ mT}$ greater than the coercivity and are marked as open squares.

Hysteresis loops were also obtained by vibrating sample magnetometry in-plane and out-of-plane at room temperature and at -195°C (shown in Figs. 2(c) and 2(d) after subtracting the substrate contribution). The saturation magnetization was around 120 kA/m at room temperature in agreement with other data on Ce:YIG thin films¹² and increased to approximately 160 kA/m at -195°C . Saturation was reached around 225 mT for both temperatures. The out-of-plane coercivity at -195°C is similar to that of the Faraday loop. By comparing the in-plane and out-of-plane loops, it is clear that the easy axis is in-plane at 25°C . At -195°C , the easy axis appears to be out-of-plane, but the in-plane loop exhibits some hysteresis which may originate from reversal influenced by the tilted $\langle 111 \rangle$ easy axes of the magnetocrystalline anisotropy. The net anisotropy field is estimated by extrapolating

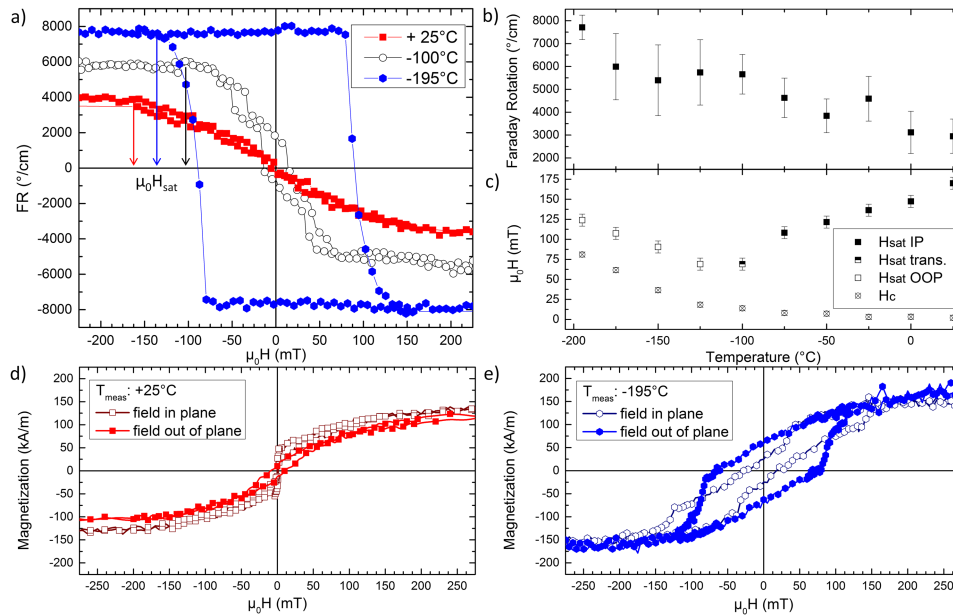


FIG. 2. Temperature dependent magnetic properties. (a) Faraday loops at 1550 nm obtained at +25 °C (red squares), –100 °C (black circles), and –195 °C (blue hexagons) for out-of-plane field. (b) The saturation FR as a function of temperature. (c) The coercive field (circles) and the saturation field (squares) measured from the out-of-plane FR loops. Filled squares correspond to an in-plane easy axis, open squares an out-of-plane easy axis, and the half-filled square a transition between them. Magnetization loops obtained at +25 °C (d) and –195 °C (e) for in-plane (open symbols) and out-of-plane (filled symbols) fields.

the zero field slope of the hard axis magnetization curve up to saturation. The resulting anisotropy fields $\mu_0 H_K = 110$ mT at 25 °C and 150 mT at –195 °C giving $|K| = 6.6$ kJ m^{–3} and 12.1 kJ m^{–3}, respectively, where $H_K = 2 K/\mu_0 M_s$.

The net anisotropy includes magnetocrystalline, magnetoelastic, and shape terms. The magnetocrystalline anisotropy term K_1 for iron garnets is typically negative favoring a $\langle 111 \rangle$ easy axis. A prior study of $\langle 100 \rangle$ Ce:YIG films gave $K_1 = -1.3$ kJ m^{–3}.¹¹ The energy difference between magnetization in a $[110]$ direction and the $[111]$ easy direction is $K_1/12$, neglecting K_2 and higher order terms.

The magnetoelastic anisotropy is uniaxial and given by $9/4 c_{44} \lambda_{111} (\pi/2 - \gamma)$ for a cubic lattice under rhombohedral distortion, where c_{44} is the shear modulus (76 GPa for YIG³⁶). YIG has negative magnetostriction, with $\lambda_{111} = -2.4 \times 10^{-6}$ at RT,³⁷ but measurements on Ce:YIG with small Ce content show that Ce provides a positive contribution to the magnetostriction. Data on Ce:YIG with 1% Ce were extrapolated to give $\lambda_{111} = +50 \times 10^{-6}$ at RT for the theoretical composition Ce₃Fe₅O₁₂,^{23,38} suggesting that our Ce_{0.59±0.18}Y_{2.86±0.41}Fe_{4.55±0.5}O₁₂ would have a small positive λ_{111} . Another report on Ce_xY_{3-x}Fe₅O₁₂ with $x = 0.05-0.125$ indicates that λ_{111} is negative but becomes smaller as the Ce content increases.^{24,38} Therefore, both the magnetoelastic anisotropy (calculated from the λ_{111} extrapolated from Ref. 24 and the measured strain) and the magnetocrystalline anisotropy favor out-of-plane easy axis, though their sum at room temperature is small, estimated ~ 4 kJ m^{–3}.

The shape anisotropy promotes an in-plane easy axis and has an estimated value of 9 kJ m^{–3} at RT based on $M_s = 120$ kA m^{–1}, corresponding to an anisotropy field of $\mu_0 H_K = 151$ mT. The measured value from Fig. 2(d) of ~ 110 mT is consistent with the dominance of the shape anisotropy and the small role played by the magnetocrystalline and magnetoelastic anisotropies at RT.

We now consider how the anisotropy terms vary with temperature. Measurements of Ce:YIG with 1% Ce showed an increase in the λ_{111} contributed by the Ce ions by a factor of 5 on cooling to liquid nitrogen temperature.²³ The magnetoelastic anisotropy is expected to increase by a similar factor, considering that the strain decreases slightly on cooling (Fig. 1(d)) but the elastic modulus increases. The temperature dependence of K_1 for Ce:YIG has not been reported, but other rare earth iron garnets show large increases in K_1 on cooling as mentioned above.^{25,26} The shape anisotropy

scales with the square of saturation magnetization and therefore also increases on cooling. However, this increase is modest: $M(-195\text{ }^\circ\text{C})/M(25\text{ }^\circ\text{C}) = 1.33$ based on our VSM data, which compares well to a published value of 1.4.¹⁴ We conclude that the increases in the sum of the magnetoelastic and magnetocrystalline anisotropies on cooling overcome the increase in shape anisotropy and drive the magnetization reorientation near $-100\text{ }^\circ\text{C}$.

Spectral dependences of FR and magnetic circular dichroism (MCD) arise from electronic transitions and therefore are related to the band structure. In particular, these dependences indicate the splitting of energy levels due to crystal field (CF). Therefore, spectral measurements of FR and MCD were obtained from a combination of spectrometers based on the azimuth modulation technique and generalized MO ellipsometry technique with a rotating analyzer covering photon energies from 0.7 to 4.4 eV which correspond to the region where the most significant optical transitions in Ce:YIG are situated. Measurements were performed in an out-of-plane magnetic field of 0.8 T to ensure saturation of the film. After subtraction of the substrate contribution, the spectra were normalized by the thickness of the film. The spectra in Fig. 3 were measured at RT and $-195\text{ }^\circ\text{C}$ and are similar to previously reported data.³⁹ Here, we focus on their differences from each other.

The infrared region is dominated by the spectroscopic structure situated near 1.4 eV (i) originating from $4f^1-4f^05d^1$ transitions in Ce^{3+} ions.⁴⁰ A rapid increase of the Faraday effect is observed at low temperatures and is typical for paramagnetic electronic transitions for which the ground state population increases at lower temperatures (also observed in Ce-doped yttrium aluminum garnet⁴⁰). A second spectroscopic structure (ii) near 1.9 eV is noticeable in the low temperature spectra. Its origin cannot be attributed to Ce^{3+} ions since the second excited state $5d^2$ is expected to be at higher energies and the spectroscopic structure has opposite sign compared to that near 1.4 eV. Moreover, the amplitude of this structure does not increase rapidly at low temperatures. Crystal field (CF) transitions of tetrahedrally and octahedrally coordinated Fe^{3+} ions have been observed around 1.9 eV in thick YIG films.⁴¹ These transitions are spin-forbidden with small oscillator strengths and should not be visible for thin films. However, a rapid increase of the neighboring Ce^{3+} transition around $-190\text{ }^\circ\text{C}$ resonantly increases the MO response around 1.9 eV, which makes this CF transition observable at low temperatures. Because tetrahedral Fe^{3+} ions have lines at least one order of magnitude more intense than those of the corresponding octahedral ions the spectroscopic structure in the MO spectra situated near 1.9 eV originates from the first tetrahedral CF transition of Fe^{3+} . Similar lines have been observed in the absorbance spectra of thick YIG films.⁴¹

Spectral behavior of the FR above 2.5 eV resembles experimental data measured on YIG films^{5,42} showing basic similarities to Bi-substituted YIG.^{5,43,44} With respect to both theoretical predictions and experimental analyses, CF and charge transfer transitions involving O $2p$ and Fe $3d$ states have been studied in detail in the spectral region between 2.4 and 4 eV^{5,44,45} (tetrahedral transitions with negative sign are marked as (iii) and (v), and the octahedral transition with positive sign is marked as (iv)). Comparing the Faraday spectra of the cooled and uncooled sample one finds a significant red-shift of peaks (iii) (of $\sim 0.04\text{ eV}$), (iv) ($\sim 0.02\text{ eV}$), and (v) (0.06 eV) with decreasing temperature. The

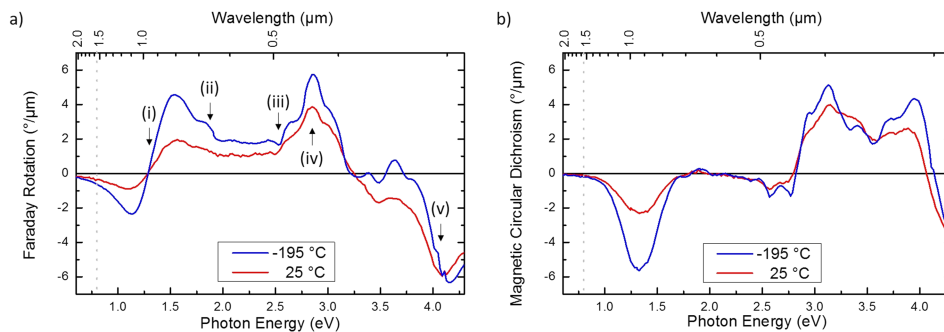


FIG. 3. Spectral dependences of (a) Faraday rotation and (b) MCD measured at liquid nitrogen and at room temperature. The applied magnetic field was 0.8 T. The dashed line corresponds to a wavelength of 1550 nm. The arrows indicating electronic transitions influenced by temperature are discussed in the main text.

lattice parameter decreases on cooling and the red-shift is related to changes in the crystallographic structure.

A similar red-shift was observed for Bi doped garnets^{5,43} but originates in the enhancement of the spectroscopic structure near 3.2 eV (visible also in Fig. 3(a) as a left shoulder of peak iv) due to the covalent interaction between Bi³⁺ and Fe³⁺ ions⁴⁵ rather than from an expansion of the lattice parameter.⁶ It is therefore crucial to look at the properties of the parent YIG material to explain the spectral shifts in the present data. Indeed, Wettling *et al.*⁴² showed a comparison of Faraday rotation spectra of YIG films at -253.15 °C and room temperature obtaining an identical red-shift.

Two factors are therefore involved in the red-shift: First, the change of the crystal field due to the temperature-induced rhombohedral lattice deformation and second, the narrowing of the transition peaks due to thermal depopulation of vibronic states built on the pure electronic ground state. The latter factor is rather straightforward. The first factor, however, needs further investigation. A rearrangement of octahedral and tetrahedral sites with the lattice contraction is suggested to explain the red-shift in the absorption spectra.⁴¹ Nevertheless, from Fig. 3 one can see that the tetrahedral sites are more susceptible to deformations ((iii) and (v)) than octahedral sites (iv).

In conclusion, Ce_{0.59±0.18}Y_{2.86±0.41}Fe_{4.55±0.5}O₁₂ films grew epitaxially on GGG substrates with an in-plane compressive strain. The unit cell geometry was analysed as a function of temperature, showing a higher thermal expansion coefficient for the Ce:YIG film compared to the GGG substrate. The film showed a reorientation from in-plane easy axis to perpendicular magnetic anisotropy upon cooling to ~ -100 °C which is attributed to increasing magnetoelastic and magnetocrystalline anisotropy energies consistent with a positive magnetostriction coefficient λ_{111} and negative K_1 . Moreover, changes in octahedral and tetrahedral arrangements due to temperature-induced lattice distortions have been observed via red-shifts of the CF transition peaks in the Faraday rotation spectra. The results suggest that the tetrahedral arrangement is more susceptible to deformations than the octahedral one.

E.L. gratefully acknowledges the German Academic Exchange Service (DAAD) for funding. The work was supported by NSF Award Nos. ECCS-1607865 and DARPA FA8650-16-1-7641. Shared experimental facilities of CMSE, an NSF MRSEC award DMR1419807, were used. The authors thank Nilanjan Chatterjee for WDS characterization and Martin Zahradnik and Charles Settens for experimental assistance.

- ¹ M. Mansuripur, "The Faraday effect," *Opt. Photonics News* **10**, 32–36 (1999).
- ² B. J. H. Stadler and T. Mizumoto, "Integrated magneto-optical materials and isolators: A review," *IEEE Photonics J.* **6**(1), 0600215 (2014).
- ³ T. Goto, M. C. Onbaşlı, and C. A. Ross, "Magneto-optical properties of cerium substituted yttrium iron garnet films with reduced thermal budget for monolithic photonic integrated circuits.," *Opt. Express* **20**(27), 28507–17 (2012).
- ⁴ S. Higuchi, Y. Furukawa, S. Takekawa, O. Kamada, K. Kitamura, and K. Uyeda, "Magneto-optical properties of cerium-substituted yttrium iron garnet single crystals for magnetic-field sensor," *Sens. Actuators, A* **105**(3), 293–296 (2003).
- ⁵ S. Wittekoek, T. J. A. Popma, J. M. Robertson, and P. F. Bongers, "Magneto-optic spectra and the dielectric tensor elements of bismuth-substituted iron garnets at photon energies between 2.2–5.2 eV," *Phys. Rev. B* **12**(7), 2777–2788 (1975).
- ⁶ M. Veis, E. Lišková, R. Antoš, Š. Višňovský, N. Kumar, D. S. Misra, N. Venkataramani, S. Prasad, and R. Krishnan, "Polar and longitudinal magneto-optical spectroscopy of bismuth substituted yttrium iron garnet films grown by pulsed laser deposition," *Thin Solid Films* **519**(22), 8041–8046 (2011).
- ⁷ T. Mizumoto, R. Takei, and Y. Shoji, "Waveguide optical isolators for integrated optics," *IEEE J. Quantum Electron.* **48**(2), 252–260, 2012.
- ⁸ M. Levy, I. Ilic, R. Scarmozzino, R. M. Osgood, R. Wolfe, C. J. Gutierrez, and G. A. Prinz, "Thin-film-magnet waveguide isolator," *IEEE Photonics Technol. Lett.* **5**(2), 198–200 (1993).
- ⁹ W. Šmigaj, J. Romero-Vivas, B. Gralak, L. Magdenko, B. Dagens, and M. Vanwolleghem, "Magneto-optical circulator designed for operation in a uniform external magnetic field," *Opt. Lett.* **35**(4), 568 (2010).
- ¹⁰ X. Y. Sun, Q. Du, T. Goto, M. C. Onbasli, D. H. Kim, N. M. Aimon, J. Hu, and C. A. Ross, "Single-step deposition of cerium-substituted yttrium iron garnet for monolithic on-chip optical isolation," *ACS Photonics* **2**(7), 856–863 (2015).
- ¹¹ A. Kehlberger, K. Richter, M. C. Onbasli, G. Jakob, D. H. Kim, T. Goto, C. A. Ross, G. Götz, G. Reiss, T. Kuschel, and M. Kläui, "Enhanced magneto-optic Kerr effect and magnetic properties of CeY₂Fe₅O₁₂ epitaxial thin films," *Phys. Rev. Appl.* **4**(1), 014008 (2015).
- ¹² M. C. Onbasli, T. Goto, X. Sun, N. Huynh, and C.A. Ross, "Integration of bulk-quality thin film magneto-optical cerium-doped yttrium iron garnet on silicon nitride photonic substrates," *Opt. Express* **22**(21), 25183 (2014).
- ¹³ T. Goto, Y. Eto, K. Kobayashi, Y. Haga, M. Inoue, and C. A. Ross, "Vacuum annealed cerium-substituted yttrium iron garnet films on non-garnet substrates for integrated optical circuits," *J. Appl. Phys.* **113**(17), 17A939 (2013).
- ¹⁴ P. Sellappan, C. Tang, J. Shi, and J. E. Garay, "An integrated approach to doped thin films with strain tunable magnetic anisotropy: Powder synthesis, target preparation and pulsed laser deposition of Bi:YIG," *Mater. Res. Lett.* **5**, 41–47 (2016).

- ¹⁵ M. Gomi, K. Satoh, H. Furuyama, and M. Abe, "Sputter deposition of Ce-substituted iron garnet films with giant magneto-optical effect," *IEEE Transl. J. Magn. Jpn.* **5**(4), 294–299 (1990).
- ¹⁶ T. Sekijima, T. Funakoshi, K. Katabe, K. Tahara, T. Fujii, K. Wakino, and M. Okada, "Growth and optical properties of Ce-substituted fibrous YIG single crystals," *Jpn. J. Appl. Phys.* **37**, 4854–4857 (1998).
- ¹⁷ A. M. Grishin and S. I. Khartsev, "Highly luminescent garnets for magneto-optical photonic crystals," *Appl. Phys. Lett.* **95**(10), 102503 (2009).
- ¹⁸ M. C. Sekhar, M. R. Singh, S. Basu, and S. Pinnepalli, "Giant Faraday rotation in $\text{Bi}_x\text{Ce}_{3-x}\text{Fe}_5\text{O}_{12}$ epitaxial garnet films," *Opt. Express* **20**(9), 9624 (2012).
- ¹⁹ Y. Suzuki, T. Goto, Y. Eto, H. Takagi, P. B. Lim, A. V. Baryshev, and M. Inoue, "Selective crystallization of magnetic garnet films on Bragg mirrors by laser annealing," *J. Magn. Soc. Jpn.* **36**(3), 183–187 (2012).
- ²⁰ S. Leitenmeier, T. Körner, J. Griesbauer, M. Herbort, A. Heinrich, and B. Stritzker, "Studies on the growth of epitaxial bismuth-substituted iron garnet on gadolinium gallium garnet single crystals by pulsed laser deposition," *J. Cryst. Growth* **310**(24), 5392–5401 (2008).
- ²¹ J. Ostoréro, M. Escorne, J. Gouzerh, and H. Le Gall, "Magneto-optical properties of Ce-Doped YIG single crystals," *J. Phys.* **IV** 7(C1), C1-719–C1-720 (1997).
- ²² T.-C. Mao and J.-C. Chen, "Influence of the addition of CeO_2 on the microstructure and the magnetic properties of yttrium iron garnet ceramic," *J. Magn. Magn. Mater.* **302**(1), 74–81 (2006).
- ²³ R. L. Comstock and J. J. Raymond, "Magnetostriction of ytterbium and cerium in YIG," *J. Appl. Phys.* **38**(9), 3737 (1967).
- ²⁴ K. P. Belov, N. V. Volkova, V. I. Raitsis, and A. Y. Chervonenkis, "Magnetostriction of cerium-substituted yttrium iron garnets," *Sov. Phys.-Solid State* **14**(6), 1850–1852 (1972).
- ²⁵ R. F. Pearson, "Magneto-crystalline anisotropy of rare-earth iron garnets," *J. Appl. Phys.* **33**(3), 1236 (1962).
- ²⁶ K. Enke, J. Fleischhauer, W. Gunßer, P. Hansen, S. Nomura, W. Tolksdorf, G. Winkler, and U. Wolfmeier, *Landolt-Börnstein Volume 12 Part A: Magnetic and Other Properties of Oxides and Related Compounds: Garnets and Perovskites* (Springer, Berlin, 1978).
- ²⁷ M. Kustov, R. Grechishkin, M. Gusev, O. Gasanov, and J. Mccord, "A novel scheme of thermographic microimaging using pyro-magneto-optical indicator films," *Adv. Mater.* **27**, 5017–5022 (2015).
- ²⁸ O. Kamada, T. Nakaya, and S. Higuchi, "Magnetic field optical sensors using Ce:YIG single crystals as a Faraday element," *Sens. Actuators, A* **119**(2), 345–348 (2005).
- ²⁹ C. Leycuras, H. Le Gall, J. Desvignes, M. Guillot, and A. Marchand, "Magnetic and magneto-optical properties of a cerium YIG single crystal," *IEEE Trans. Magn.* **21**(5), 1660–1662 (1985).
- ³⁰ T. B. Mitchell and P. E. Wigen, "The Faraday rotation of bismuth and thulium-substituted yttrium iron garnet," *J. Appl. Phys.* **61**(8), 3259–3261 (1987).
- ³¹ Y. Xu, J. H. Yang, and X. J. Zhang, "Quantum theory of the strong magneto-optical effect of Ce-substituted yttrium iron garnet," *Phys. Rev. B* **50**(18), 428–434 (1994).
- ³² N. B. Ibrahim, C. Edwards, and S. B. Palmer, "Pulsed laser ablation deposition of yttrium iron garnet and cerium-substituted YIG films," *J. Magn. Magn. Mater.* **220**(2), 183–194 (2000).
- ³³ J. Rongjin, Y. Wenhui, F. Caixiang, and Z. Yanwei, "synthesis of heavily Ce-doped YIG nanocrystals and their microstructures and magnetic properties," *J. Mater. Chem. C* **1**(9), 1763 (2013).
- ³⁴ P. Mukhopadhyay, "High- T_c films on GGG substrates," *Supercond. Sci. Technol.* **7**(5), 298–299 (1994).
- ³⁵ L. Bi, *Magneto-Optical Oxide Thin Films and Integrated Nonreciprocal Photonic Devices*, Ph.D. thesis, Massachusetts Institute of Technology, 2011.
- ³⁶ Y. A. Burenkov and S. P. Nikanorov, "Temperature effect on the elastic properties of yttrium garnet ferrite $\text{Y}_3\text{Fe}_5\text{O}_{12}$," *Phys. Solid State* **44**(2), 318–323 (2002).
- ³⁷ J. R. Patel, K. A. Jackson, and J. F. Dillon, Jr., "X-ray topographic and optical observations of magnetic domains in yttrium iron garnet (YIG)," *J. Appl. Phys.* **39**(8), 3767 (1968).
- ³⁸ H. P. J. Wijn, *Garnets* (Springer-Verlag, Berlin, Heidelberg, 1991), Vol. 27e.
- ³⁹ M. C. Onbasli, L. Beran, M. Zahradník, M. Kučera, R. Antoš, J. Mistrik, G. F. Dionne, M. Veis, and C. A. Ross, "Optical and magneto-optical behavior of cerium yttrium iron garnet thin films at wavelengths of 200–1770 nm," *Sci. Rep.* **6**, 23640 (2016).
- ⁴⁰ M. Kucera, J. Bok, and K. Nitsch, "Faraday rotation and MCD in Ce doped," *Solid State Commun.* **69**(11), 1117–1121 (1989).
- ⁴¹ D. L. Wood and J. P. Remeika, "Effect of impurities on the optical properties of yttrium iron garnet," *J. Appl. Phys.* **38**(3), 1038–1045 (1967).
- ⁴² W. Wettling, B. Andlauer, P. Koidl, J. Schneider, and W. Tolksdorf, "Optical absorption and Faraday rotation in yttrium iron garnet," *Phys. Status Solidi. B* **59**(1), 63–70 (1973).
- ⁴³ M. Y. Chern, F. Y. Lo, D. R. Liu, K. Yang, and J. Sen Liaw, "Red shift of Faraday rotation in thin films of completely bismuth-substituted iron garnet $\text{Bi}_3\text{Fe}_5\text{O}_{12}$," *Jpn. J. Appl. Phys.* **38**(12A), 6687–6689 (1999).
- ⁴⁴ M. Deb, E. Popova, A. Fouchet, and N. Keller, "Magneto-optical Faraday spectroscopy of completely bismuth-substituted $\text{Bi}_3\text{Fe}_5\text{O}_{12}$ garnet thin films," *J. Phys. D: Appl. Phys.* **45**(45), 455001 (2012).
- ⁴⁵ G. F. Dionne and G. A. Allen, "Molecular-orbital analysis of magneto-optical Bi–O–Fe hybrid excited states," *J. Appl. Phys.* **75**(10), 6372–6374 (1994).